Nonadditivity of van der Waals forces on liquid surfaces

Prashanth S. Venkataram, Jeremy D. Whitton, and Alejandro W. Rodriguez

Phys. Rev. E **94**, 030801 — Published 22 September 2016

DOI: 10.1103/PhysRevE.94.030801

Non-additivity of van der Waals forces on liquid surfaces

Prashanth S. Venkataram,[1] Jeremy D. Whitton,[2] and Alejandro W. Rodriguez[1]

[1]*Princeton University, Department of Electrical Engineering, Princeton, New Jersey 08544, USA*
[2]*Princeton University, Department of Physics, Princeton, New Jersey 08544, USA*

(Dated: August 12, 2016)

We present an approach for modeling nanoscale wetting and dewetting of textured solid surfaces that exploits recently developed, sophisticated techniques for computing exact long-range dispersive van der Waals (vdW) or (more generally) Casimir forces in arbitrary geometries. We apply these techniques to solve the variational formulation of the Young–Laplace equation and predict the equilibrium shapes of liquid–vacuum interfaces near solid gratings. We show that commonly employed methods of computing vdW interactions based on additive Hamaker or Derjaguin approximations, which neglect important electromagnetic boundary effects, yield large discrepancies in the shapes and behaviors of such liquid surfaces compared to exact methods.

Wetting and dewetting phenomena are ubiquitous in soft matter systems and have a profound impact on many disciplines, including biology [1], microfluidics [2], and microfabrication [3]. One problem of great interest concerns the suspension of fluid films on or near structured surfaces where, depending on the interplay of competing short-range molecular or capillary forces (e.g. surface tension), gravity, and long-range dispersive interactions (i.e. van der Waals or more generally, Casimir forces), the film may undergo wetting or dewetting transitions, or exist in some intermediate state, forming a continuous surface profile of finite thickness [2, 4]. Thus far, theoretical analyses of these competing effects have relied on ad-hoc, approximate descriptions of long-range dispersive van der Waals (vdW) forces [5–7], i.e. so-called Derjaguin [8] and Hamaker [9] approximations, based on additive interactions (defined further below) which can fail dramatically when applied outside of their narrow range of validity, i.e. dilute media or gently curved surfaces [5, 10–12].

In this paper, building on recently developed theoretical techniques for computing Casimir forces in arbitrary geometries [13, 14], we consider an approach for studying the equilibrium shapes of liquid surfaces that captures the full, long-range vdW interactions between interfaces (no approximations) [15]. We quantify the degree to which additive approximations can fail in this context by considering a proof of concept system, consisting of two perfect electrically conducting (PEC) surfaces interacting through vacuum [Fig. 1], with the upper and lower surfaces playing the role of a fixed solid grating and an idealized deformable fluid, respectively. In particular, we show that the competition between surface tension and vdW pressure (as computed by our exact methods) leads to quantitatively and qualitatively different liquid shapes, as well as dramatically different contact transitions, compared with predictions based on commonly employed, additive approximations. Our choice of PEC surfaces allows for a scale-invariant analysis of the role of geometry on fluid deformations, ignoring effects associated with material dispersion that would otherwise complicate our analysis and are likely to result in even larger deviations [5, 16]. Our results demonstrate the need for accurate calculations of vdW effects in experimental studies of fluid suspensions at the nanometer scale.

Equilibrium fluid problems are typically studied by way of the augmented Young-Laplace equation [17],

$$\gamma\nabla\cdot\left(\frac{\nabla\Psi}{\sqrt{1+|\nabla\Psi|^2}}\right)+\frac{\delta}{\delta\Psi}\left(\mathcal{E}_{\rm other}[\Psi]+\mathcal{E}_{\rm vdW}[\Psi]\right)=0 \tag{1}$$

describing the local balance of forces (variational derivatives of energies) acting on a fluid of surface profile $\Psi(\mathbf{x})$. The first two terms describe surface and other external forces (e.g. gravity), with γ denoting the fluid–vacuum surface tension, while the third term $\frac{\delta}{\delta\Psi}\mathcal{E}_{\rm vdW}$ denotes the local disjoining pressure arising from the changing vdW fluid–substrate interaction energy $\mathcal{E}_{\rm vdW}$. Semi-analytical [18, 19] and brute-force [20, 21] solutions of the YLE have been pursued in order to examine various classes of wetting problems, including those arising in atomic force microscopy, wherein a solid object (e.g. spherical tip) is brought into close proximity to a fluid surface [18–20], or those involving liquids on chemically [22, 23] or physically [2, 4, 21] textured surfaces.

While in principle the vdW pressure on a fluid surface can be obtained via atomistic calculations, such an approach is very difficult to carry out except at sub-nanometric scales [5]. At larger lengthscales where the optical response of materials can be described through macroscopic dielectric functions, the complicated screening of charge fluctuations and ensuing vdW or Casimir interactions and their dependence on material and geometric parameters is accurately captured via the complex electromagnetic modes and scattering properties of surfaces [5]. The first accurate calculations of such interactions were carried out decades ago in simple, planar geometries, either by summing the zero-point energies of electromagnetic fields [24] or via modern macroscopic fluctuational electrodynamics techniques [5, 15, 25, 26] that have been recently generalized to encompass more complex geometries [5].

A commonality among prior theoretical studies of (1) that attempt to capture vdW-induced surface deformations is the use of simple, albeit heuristic approximations that treat vdW interactions as additive forces that often depend on the shape of the fluid surface in some power-law fashion [8, 9, 27]. One such approach is known as the Hamaker or pairwise-summation (PWS) approximation [9], which models the vdW interaction between two macroscopic surfaces via the pairwise summation of volumetric elements interacting through dipolar London–vdW or Casimir–Polder [28, 29] forces. While PWS

resembles and builds on the familiar vdW picture of molecular or dipolar dispersive interactions, and hence offers conceptual simplicity, when applied to complicated structures, it neglects the interplay of electrodynamic screening and multiple-scattering effects in complex geometries [5], and is highly limited in scope to situations involving dilute media [11]. A more sophisticated but equally ad-hoc approach is the so-called Derjaguin or proximity-force approximation (PFA) [8, 27], which models the interaction between nearby surfaces as additive line-of-sight interactions between infinitesimal, planar surface elements (computed via the so-called Lifshitz formula [25]), and is highly limited to situations involving objects with gently curved, proximate surfaces [5]. Ultimately, both of these approximations assume some notion of additivity, with the force resulting from the cumulative force contributions of either surface or dipolar interactions. In contrast, exact calculations of vdW forces capture the "dressed" electromagnetic response of fluctuating dipoles stemming from the highly shape-dependent boundary conditions of the electromagnetic fields. The discrepancy between such additive approximations and exact calculations is often referred to as the non-additivity of the vdW interaction.

More recently, powerful electrodynamic scattering methods (detailed in recent reviews [5, 15, 26]) have been developed to compute *exact* vdW interactions, illustrating the failure of additive approximations in non-planar geometries, e.g. demonstrating non-monotonic, logarithmic, and even repulsive interactions in more complex geometries [5, 15, 30, 31]. These brute-force techniques share little semblance with additive approximations, with the exact vdW energy in these modern formulations often cast as a log-determinant expression involving the full (no approximations) electromagnetic scattering properties of the individual objects, obtained semi-analytically or numerically by exploiting spectral or localized basis expansions of the scattering unknowns [5, 32]. The generality of these methods does, however, come at a price, with even the most sophisticated of formulations requiring thousands or hundreds of thousands of scattering calculations to be performed [5]. Despite the fact that fluid suspensions motivated much of the original theoretical work on vdW interactions between macroscopic bodies [6, 7, 25, 33], to our knowledge this paper is the first to apply these exact techniques to wetting problems where non-additivity and boundary effects play a significant role in fluid surface deformations.

Methods.– In order to solve (1) in general settings, we require knowledge of $\frac{\delta}{\delta\Psi}\mathcal{E}_{\rm vdW}[\Psi]$ for arbitrary Ψ. We employ a mature and freely available method for computing vdW interactions in arbitrary geometries and materials [34, 35], based on the fluctuating–surface current (FSC) framework [13, 14]. FSC is based on the surface integral equation (SIE) formulation of Maxwell's equations in arbitrary piecewise-homogeneous geometries such as the one that we consider, and is most efficient when surface unknowns are expanded in terms of basis functions $\mathbf{f}^{(\alpha)}(\mathbf{x})$ supported on localized triangular mesh elements on the material interfaces [Fig. 1(a)], making it a boundary element method (BEM). Using the vacuum dyadic Green's function $\mathbf{\Gamma}^{(0)}$, FSC computes $M_{\alpha\beta} = \int \mathbf{f}^{(\alpha)} \cdot (\mathbf{\Gamma}^{(0)} \star \mathbf{f}^{(\beta)})$ at each frequency; $\mathbb{M}$, known as the BEM matrix, is akin to a scattering matrix, coupling the different basis functions via $\mathbf{\Gamma}^{(0)}$. FSC then employs the fluctuation–dissipation theorem to connect the vdW energy to the full Green's function, and analytically evaluates the spatial integrals of the Green's function to yield

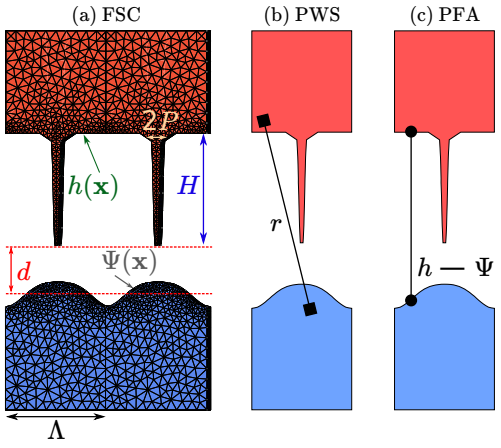

Figure 1. Schematic of fluid–grating geometry comprising a fluid (blue) of surface profile $\Psi(\mathbf{x})$ in close proximity (average distance d) to a solid grating (red) of height profile $h(\mathbf{x})$, involving thin nanorods of height H, thickness $2P$, and period Λ. (a) Representative mesh employed by a recently developed FSC boundary-element method [34] for computing exact vdW energies in complex geometries. (b) and (c) illustrate commonly employed pairwise–summation (PWS) and proximity–force approximations (PFA), involving volumetric and surface interactions throughout the bodies, respectively.

$$\mathcal{E}_{\rm FSC} = \frac{\hbar}{2\pi}\int_0^\infty {\rm d}\xi\ \ln(\det(\mathbb{M}\mathbb{M}_\infty^{-1})) \qquad (2)$$

where $\mathbb{M}$ is defined above, $\mathbb{M}_\infty$ is the evaluation of $\mathbb{M}$ when the objects are infinitely separated, and the integration is over imaginary frequencies $\xi = {\rm i}\omega$. Because exact methods most commonly yield the total vdW energy or force, rather than the local pressure on Ψ, it is convenient to consider the YLE in terms of an equivalent variational problem that minimizes the total energy functional [36, 37],

$$\mathcal{E}[\Psi] = \gamma\int\sqrt{1+|\nabla\Psi|^2} + \mathcal{E}_{\rm other}[\Psi] + \mathcal{E}_{\rm vdW}[\Psi], \qquad (3)$$

where just as in (1), the first term captures the surface energy, the second captures contributions from gravity or bulk thermodynamic/fluid interactions [19, 20], and the third captures the dispersive vdW interaction energy. For simplicity, we focus only on the impact of surface and dispersive vdW interactions, thereby setting $\mathcal{E}_{\rm other} = 0$; additionally, since the surface curvatures we consider are small compared to the Tolman length [38], we ignore higher-order corrections to γ, taking it to be constant as Ψ varies.

Equation 3 can be solved numerically via any number of available nonlinear optimization/minimization techniques [36, 37], requiring only a convenient parametrization of Ψ using a finite number of degrees of freedom. In what follows, we consider numerical solution of (3) for the particular

case of a deformable incompressible PEC surface Ψ interacting through vacuum with a 1d-periodic PEC grating of period Λ and shape $h(\mathbf{x}) = d - H\left(\frac{1}{e^{\alpha(x-P)}+1} + \frac{1}{e^{-\alpha(x+P)}+1} - 2\right)$, for $|x| < \frac{\Lambda}{2}$, with half-pitch $P = 0.03\Lambda$ and height $H = 1.2\Lambda$, representing a rectangular grating whose period and pitch can be independently tuned to provide large aspect ratios and curvatures that are likely to break the assumptions underlying PWS and PFA. Figure 1 shows the grating surface and fluid profile obtained by solving (3) for a representative set of parameters and mesh discretization. Here, $d = 0.4\Lambda$ is the initial minimum grating-fluid separation, and $\alpha\Lambda = 150$ is a parameter that smoothens otherwise sharp corners in the grating, alleviating spatial discretization errors in the calculation of $\mathcal{E}_{\rm vdW}$ while having a negligible impact on the qualitative behavior of the energy compared to what one might expect from more typical, piecewise-constant gratings [10].

To minimize the energy, we employ free implementations of the COBYLA and BOBYQA local derivative-free optimization algorithms found in the NLOPT optimization suite [39–41]. Although the localized basis functions or mesh of the FSC method provide one possible parametrization of the surface, for the class of periodic problems explored here, a simple Fourier expansion of the surface provides a far more efficient and convenient basis, requiring far fewer degrees of freedom to describe a wide range of periodic shapes. Because the grating is translationally invariant along the z direction and mirror-symmetric about $x = 0$, we parametrize Ψ in terms of a cosine basis, $\Psi(\mathbf{x}) = \sum_n c_n \cos\left(\frac{2\pi n x}{\Lambda}\right)$, with the finite number of coefficients $\{c_n\}$ functioning as minimization parameters. As we show below, this choice not only offers a high degree of convergence, requiring typically less than a dozen coefficients, but also automatically satisfies the incompressibility or volume-conservation condition $\int \Psi = 0$, which would otherwise require an additional, nonlinear constraint. Note that the optimality and efficiency of the minimization can be significantly improved when local derivative information (with respect to the minimization parameters) is available, but given that even a single evaluation of $\mathcal{E}_{\rm vdW}[\Psi]$ is expensive—a tour-de-force calculation involving hundreds of scattering calculations [5]—this is currently prohibitive in the absence of an adjoint formulation (a topic of future work) [42]. Given our interest in equilibrium fluid shapes close to the initial condition of a flat fluid surface ($\Psi = 0$) and because of the small number of degrees of freedom $\{c_n\}$ needed to resolve the shapes, we find that local, derivative-free optimization is sufficiently effective, yielding fast-converging solutions.

In what follows, we compare the solutions of (3) based on (2) against those obtained through PFA and PWS, which approximate $\mathcal{E}_{\rm vdW}$ in this periodic geometry as:

$$\mathcal{E}_{\rm PFA} = -\frac{\pi^2\hbar c}{720}\int_{-\Lambda/2}^{\Lambda/2} \mathrm{d}x \left(\frac{1}{h(x)-\Psi(x)}\right)^3 \qquad (4)$$

$$\mathcal{E}_{\rm PWS} = A\int_{-\Lambda/2}^{\Lambda/2}\mathrm{d}x'\int_{-\infty}^{\infty}\mathrm{d}x\int_{h(x')}^{\infty}\mathrm{d}y'\int_{-\infty}^{\Psi(x)}\mathrm{d}y\frac{1}{s^6}, \qquad (5)$$

where $A = -\frac{2\pi\hbar c}{45}$ is a Hamaker-like coefficient obtained by requiring that (5) yield the correct vdW energy for two parallel PEC plates, as is typically done [43]. Equation 5 is obtained from pairwise integration of the r^{-7} Casimir–Polder interactions following integration over z and z', with $r = \sqrt{s^2 + (z-z')^2}$ and $s = \sqrt{(x-x')^2 + (y-y')^2}$ [44]. Note that because we only consider perfect conductors and there is no dispersion, all results can be quoted in terms of an arbitrary length scale, which we choose to be Λ. Additionally, we express the surface tension γ in units of $\gamma_{\rm vdW} = \frac{\pi^2\hbar c}{720 d^3}$, the vdW energy per unit area between two flat PEC plates separated by distance d.

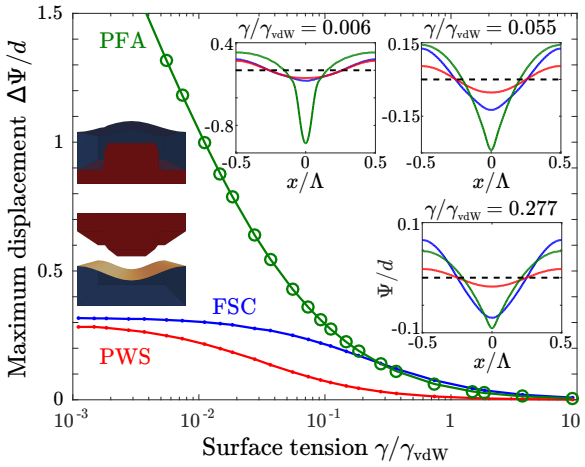

Figure 2. Maximum displacement $\Delta\Psi/d$ of a fluid–vacuum interface that is repelled from a grating (insets) by a repulsive vdW force, as a function of surface tension $\gamma/\gamma_{\rm vdW}$, obtained via solution of (3) using FSC (blue), PWS (red), and PFA (green) methods. Circles indicate results obtained through (1). Insets show the equilibrium fluid–surface profiles at selected $\gamma \in \{0.006, 0.055, 0.277\}\gamma_{\rm vdW}$, with the unperturbed $\Psi = 0$ surface denoted by black dashed lines.

In what follows, we consider the equilibrium fluid shapes under both repulsive [Fig. 2] or attractive [Fig. 3] vdW pressures: for our simplified model of PEC surfaces interacting through vacuum, this is achieved through an appropriate sign choice for $\mathcal{E}_{\rm vdW}$. In either case, we consider local optimizations with small initial trust radii around $\Psi = 0$, and characterize the equilibrium fluid profile $\Psi(x)$ as γ is varied. For each γ, the optimization calculations take a few minutes with a single processor core to converge under the additive models of vdW interactions; by contrast, under our FSC method for computing vdW interactions, the optimization calculations take over 24 hours, even with parallelization over six processor cores, demonstrating the vastly increased computational complexity of our exact method over prior approximate methods. Our minimization approach is also validated against numerical solution of (1) under PFA (green circles).

Repulsion.– We first consider the effects of vdW repulsion on the equilibrium profile of the fluid–vacuum interface, enforced in our PEC model by flipping the sign of the otherwise attractive vdW energy; this is not physically realizable for smooth PEC surfaces interacting through vacuum, but captures the influence of geometry on the repelled fluid inter-

face [Fig. 2(insets)]. Such a situation arises commonly in realistic fluids whenever the fluid and grating dielectric dispersions satisfy the Dzyaloshinskii–Lifshitz–Pitaevskii (DLP) criterion [6, 25] for repulsion. Figure 2 compares the dependence of the maximum displacement $\Delta\Psi = \Psi_{\max} - \Psi_{\min}$ of the fluid surface on γ, as computed by FSC (blue), PWS (red), and PFA (green). Also shown are selected surface profiles at small, intermediate, and large $\gamma/\gamma_{\rm vdW}$. Note that the combination of a repulsive vdW force, surface tension, and incompressibility leads to a *locally stable* equilibrium shape.

Under large γ, the surface energy dominates and thus all three methods result in nearly-flat profiles, with $|\Psi| \ll d$. While both additive approximations reproduce the exact energy of the plane–plane geometry (with the unnormalized PWS energy underestimating the exact energy by 20% [11]), we find that (at least for this particular grating geometry) $\mathcal{E}_{\rm PWS,PFA}/\mathcal{E}_{\rm FSC} \approx 0.25$ in the limit $\gamma \to \infty$, revealing that even for a flat fluid surface, the grating structure contributes significant non-additivity. Noticeably, at large but finite $\gamma \gg \gamma_{\rm vdW}$, $\Delta\Psi$ is significantly larger under FSC and PFA than under PWS, with $\Psi_{\rm FSC,PWS}$ exhibiting increasingly better qualitative and quantitative agreement compared to the sharply peaked $\Psi_{\rm PFA}$ as γ decreases [Fig. 2(insets)]. The stark deviation of PFA from FSC and PWS in the vdW–dominated regime $\gamma \ll \gamma_{\rm vdW}$ is surprising in that PWS involves volumetric interactions within the objects, whereas PFA and FSC depend only on surface topologies. Essentially, the pointwise nature of PFA means $\mathcal{E}_{\rm PFA}$ depends only on the local surface–surface separation, decreasing monotonically with decreasing separations and competing with surface tension and incompressibility to yield a surface profile that nearly replicates the shape of the grating in the limit $\gamma \to 0$. Quantitatively, PFA leads to larger $\Delta\Psi$ as $\gamma \to 0$, asymptoting to a constant $\lim_{\gamma\to 0}\Delta\Psi_{\rm PFA} \to H = 3d$ at significantly lower $\frac{\gamma}{\gamma_{\rm vdW}} < 10^{-5}$. On the other hand, both $\mathcal{E}_{\rm FSC}$ and $\mathcal{E}_{\rm PWS}$ exhibit much weaker dependences on the fluid shape at low γ, with the former depending slightly more strongly on the surface amplitude and hence leading to asymptotically larger $\Delta\Psi$ as $\gamma \to 0$; in this geometry, we find that $\Delta\Psi_{\rm FSC,PWS} \to \{0.32, 0.28\}d$ for $\frac{\gamma}{\gamma_{\rm vdW}} \lesssim 10^{-2}$. Furthermore, while PFA and PWS are found to agree with FSC at large and small γ, respectively, neither approximation accurately predicts the surface profile in the intermediate regime $\gamma \sim \gamma_{\rm vdW}$, where neither vdW nor surface energies dominate. Ultimately, neither of these approximations is capable of predicting the fluid shape over the entire range of γ.

Attraction.– We now consider the effects of vdW attraction, arising in our idealized model through the interaction between the PEC liquid–vacuum and grating surfaces. Such a situation is realized whenever the dielectric properties of fluids on or near structures [Fig. 3(insets)] satisfy the DLP criterion for attraction [6, 25]. Here, in contrast to the case of repulsion, matters are complicated by the fact that $\mathcal{E}_{\rm vdW} \to -\infty$ as the fluid interface approaches the grating, leading to a fluid instability or contact transition below some critical $\gamma^{(\rm c)}$, depending on the competition between the restoring surface tension and attractive vdW pressure. Such instabilities have been studied in microfluidic systems through both additive approximations [2, 4, 18, 45], but as we show in Fig. 3, non-additivity can lead to dramatic quantitative discrepancies in the predictions obtained from each method of computing $\mathcal{E}_{\rm vdW}$. To obtain $\gamma^{(\rm c)}$ along with the shape of the fluid surface for $\gamma > \gamma^{(\rm c)}$, we seek the nearest local solution of (3) starting from $\Psi = 0$. Figure 3 quantifies the onset of the contact transition by showing the variation of the minimum grating-fluid separation $h_{\min} - \Psi_{\max}$ with respect to γ, as computed by FSC (blue), PWS (red), and PFA (green), along with the corresponding $\mathcal{E}_{\rm vdW}$ [Fig. 3(inset)] normalized to their respective values for the plane–grating geometry (attained in the limit $\gamma \to \infty$). Also shown in the top-right inset are the optimal surface profiles at $\gamma \approx \gamma^{(\rm c)}$ obtained from the three methods.

In contrast to the case of repulsion, here the fluid surface approaches rather than moves away from the grating, which changes the scaling of $\mathcal{E}_{\rm vdW}$ with respect to Ψ, thereby leading to very different qualitative results. In particular, we find that $\mathcal{E}_{\rm FSC}$ exhibits a much stronger dependence on $h_{\min} - \Psi_{\max}$ compared to PWS and PFA, leading to a much larger $\gamma^{(\rm c)}$ and a correspondingly broad surface profile; given that the strong curvature and large aspect ratio of the grating profile violates the assumptions underlying PWS and PFA, this behavior cannot be gleaned from a simple power-law or asymptotic correction to additive approximations, but can only be captured by an exact numerical computational method like our FSC method. As before, the strong dependence of $\mathcal{E}_{\rm PFA}$ on the fluid surface, a consequence of the pointwise nature of the approximation, produces a sharply peaked surface profile, while the very weak dependence of $\mathcal{E}_{\rm PWS}$ on the fluid shape ensures both a gross underestimation of $\gamma^{(\rm c)}$ along with a broader surface profile. Most interestingly, we find that $\gamma^{(\rm c)}_{\rm FSC,PFA,PWS} \approx \{0.65, 0.38, 0.07\}\gamma_{\rm vdW}$, emphasizing the failure of PWS to capture the critical surface tension by nearly an order of magnitude.

Concluding Remarks.– The predictions and approach described above offer evidence of the need for exact vdW calculations for the accurate determination of equilibrium fluid behaviors on or near structured surfaces. While we chose to employ a simple materials-agnostic and scale-invariant model for the vdW energy, realistic (dispersive) materials can be readily analyzed within the same formalism, requiring no modifications. Recent works [11, 16] have shown that additive approximations applied to even simpler structures can contribute larger discrepancies in dielectric as opposed to PEC bodies. Given this, we expect to see even larger differences owing to non-additivity when complex materials and geometries are considered together. In particular, we anticipate for complex periodic geometries like the one we have studied that in situations involving a contact transition, namely either a thin liquid film on or a bulk fluid separated in vacuum from a solid grating, with the liquid surface tension varied through appropriate use of surfactants in either case, PWS and PFA could underestimate the critical surface tension by over 50%, while our exact method could provide more accurate agreement with experimental studies of contact transitions in such systems. We further anticipate employing our exact method to study extensions of the original liquid He^4 wetting experiments that motivated the development of the general Lifshitz

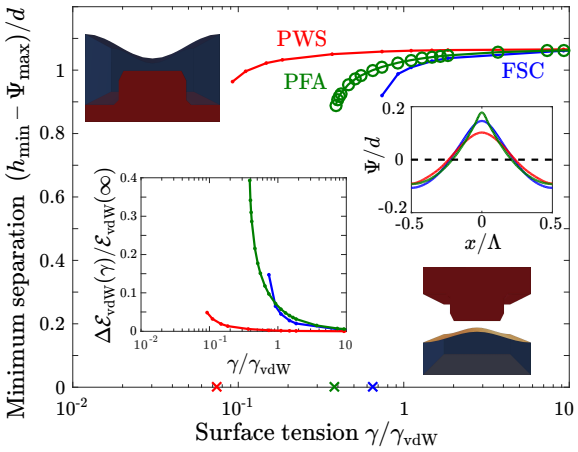

Figure 3. Minimum surface–surface separation $\frac{h_{\min}-\Psi_{\max}}{d}$ of a fluid–vacuum interface that is attracted to a grating (insets) by an attractive vdW force, as a function of surface tension $\frac{\gamma}{\gamma_{\rm vdW}}$, obtained via solution of (3) using FSC (blue), PWS (red), and PFA (green) methods. Circles indicate results obtained through (1). Contact transitions occurring at critical values of surface tension $\gamma^{(\rm c)}$, marked as 'x'. The top-right inset shows the equilibrium fluid–surface profiles near $\gamma^{(\rm c)}$ while the bottom-left inset shows the relative changes in the equilibrium vdW energies from the energies of the unperturbed ($\Psi = 0$) plane–grating geometry (the limit of $\gamma \to \infty$).

theory in the first place [25].

[1] S. Prakash, M. Pinti, and B. Bhushan, Philosophical Transactions of the Royal Society of London A: Mathematical, Physical and Engineering Sciences **370**, 2269 (2012).
[2] M. Geoghegan and G. Krausch, Progress in Polymer Science **28**, 261 (2003).
[3] S. Chakraborty, "Microfluidics and microfabrication," (Springer US, 2010) Chap. 3, pp. 113–130.
[4] D. Bonn, J. Eggers, J. Indekeu, J. Meunier, and E. Rolley, Reviews of Modern Physics **81**, 739 (2009).
[5] L. M. Woods, D. A. R. Dalvit, A. Tkatchenko, P. Rodriguez-Lopez, A. W. Rodriguez, and R. Podgornik, arXiv preprint **28**, 261 (2015).
[6] J. N. Israelachvili, *Intermolecular and Surface Forces (Third Edition)*, third edition ed. (Academic Press, San Diego, 2011).
[7] V. A. Parsegian, *Van der Waals Forces* (Cambridge University Press, 2005).
[8] B. Derjaguin, Kolloid-Zeitschrift **69**, 155 (1934).
[9] H. Hamaker, Physica **4**, 1058 (1937).
[10] R. Büscher and T. Emig, Phys. Rev. A **69**, 062101 (2004).
[11] A.-F. Bitbol, A. Canaguier-Durand, A. Lambrecht, and S. Reynaud, Phys. Rev. B **87**, 045413 (2013).
[12] T. Emig, A. Hanke, R. Golestanian, and M. Kardar, Phys. Rev. Lett. **87**, 260402 (2001).
[13] M. T. H. Reid, J. White, and S. G. Johnson, Phys. Rev. A **88**, 022514 (2013).
[14] M. T. H. Reid, A. W. Rodriguez, J. White, and S. G. Johnson, Phys. Rev. Lett. **103**, 040401 (2009).
[15] A. W. Rodriguez, P.-C. Hui, D. P. Woolf, S. G. Johnson, M. Lončar, and F. Capasso, Annalen der Physik **527**, 45 (2015).
[16] C. Noguez and C. E. Román-Velázquez, Phys. Rev. B **70**, 195412 (2004).
[17] J. C. Berg, "An introduction to interfaces & colloids: The bridge to nanoscience," (World Scientific, 2010) Chap. 2, pp. 23–106.
[18] D. B. Quinn, J. Feng, and H. A. Stone, Langmuir **29**, 1427 (2013).
[19] R. Ledesma-Alonso, D. Legendre, and P. Tordjeman, Phys. Rev. Lett. **108**, 106104 (2012).
[20] R. Ledesma-Alonso, P. Tordjeman, and D. Legendre, Phys. Rev. E **85**, 061602 (2012).
[21] J. B. Sweeney, T. Davis, and L. E. Scriven, Langmuir **9**, 1551 (1993).
[22] C. Bauer and S. Dietrich, Phys. Rev. E **60**, 6919 (1999).
[23] A. Checco, O. Gang, and B. M. Ocko, Phys. Rev. Lett. **96**, 056104 (2006).
[24] H. B. G. Casimir, Proc. K. Ned. Akad. Wet. **51**, 793 (1948).
[25] I. E. Dzyaloshinskii, E. M. Lifshitz, and L. P. Pitaevskii, Advances in Physics **10**, 165 (1961).
[26] A. W. Rodriguez, F. Capasso, and S. G. Johnson, Nature Photonics **5**, 211 (2011).
[27] B. V. Derjaguin, I. I. Abrikosova, and E. M. Lifshitz, Q. Rev. Chem. Soc. **10**, 295 (1956).
[28] H. B. G. Casimir and D. Polder, Physical Review **73**, 360 (1948).
[29] A. D. McLachlan, Proceedings of the Royal Society of London A: Mathematical, Physical and Engineering Sciences **271**, 387 (1963).
[30] A. Rodriguez, M. Ibanescu, D. Iannuzzi, F. Capasso, J. D. Joannopoulos, and S. G. Johnson, Phys. Rev. Lett. **99**, 080401 (2007).
[31] M. Bordag, Phys. Rev. D **73**, 125018 (2006).
[32] A. Lambrecht, P. A. M. Neto, and S. Reynaud, New Journal of Physics **8**, 243 (2006).
[33] S. K. Lamoreaux, Phys. Today.

[34] M. T. Homer Reid and S. G. Johnson, ArXiv e-prints (2013), arXiv:1307.2966 [physics.comp-ph].
[35] http://homerreid.com/scuff-EM.
[36] E. Bormashenko, Langmuir **25**, 10451 (2009).
[37] D. Silin and G. Virnovsky, Transport in Porous Media **82**, 485 (2009).
[38] H. M. Lu, , and Q. Jiang, Langmuir **21**, 779 (2005).
[39] Steven G. Johnson, The NLopt nonlinear-optimization package, http://ab-initio.mit.edu/nlopt.
[40] M. J. D. Powell, "A direct search optimization method that models the objective and constraint functions by linear interpolation," in Advances in Optimization and Numerical Analysis, eds. S. Gomez and J.-P. Hennart (Kluwer Academic: Dordrecht, 1994), p. 51-67.
[41] M. J. D. Powell, "The BOBYQA algorithm for bound constrained optimization without derivatives," Department of Applied Mathematics and Theoretical Physics, Cambridge England, technical report NA2009/06 (2009).
[42] M. B. Giles and N. A. Pierce, Flow, Turbulence and Combustion **65**, 393 (2000).
[43] L. Bergström, Advances in Colloid and Interface Science **70**, 125 (1997).
[44] Note that in situations involving a deformed PEC surface and flat PEC plate, one can show that $\mathcal{E}_{\rm PWS} = \mathcal{E}_{\rm PFA}$ [46], a consequence of the additivity of the interaction.
[45] T. Kerle, R. Yerushalmi-Rozen, J. Klein, and L. J. Fetters, Europhys. Lett. **44**, 484 (1998).
[46] T. Emig, A. Hanke, R. Golestanian, and M. Kardar, Phys. Rev. A **67**, 022114 (2003).